Hindawi Publishing Corporation
International Journal of Antennas and Propagation
Volume 2014, Article ID 958148, 18 pages
http://dx.doi.org/10.1155/2014/958148

Research Article

A Generalized Approach for Computation of Near Field Radiation Pattern of an Antenna

Preetham Shankpal,[1] Varun Arur,[1] Govind Kadambi,[1] and James Shuttleworth[2]

[1] *M. S. Ramaiah School of Advanced Studies, India*
[2] *Department of Computing and Digital Environment, School of Engineering, Coventry University, Coventry, UK*

Correspondence should be addressed to Varun Arur; varunarur@gmail.com

Received 24 March 2014; Revised 23 July 2014; Accepted 24 July 2014; Published 19 October 2014

Academic Editor: Ahmad Safaai-Jazi

A generalized procedure in the form of an analytical formulation for the determination of radiation pattern of an antenna at any arbitrary distance which covers the near field as well as far field is presented in this paper. With the prior knowledge of either the current or field distribution on the radiating aperture, the proposed near field analysis is generic and can be applied for wide variety of antenna elements. The underlying principle of the generalized procedure is tantamount to considering the radiating aperture as an array of point electric and magnetic dipoles. The validity and novelty of the proposed new approach have been substantiated considering an open ended circular cylindrical waveguide and a conical horn as case studies and treating the far field as a special case of near field with pertinent distance criterion. The effect of change in the distance of observation ranging from reactive near field to far field on the radiation patterns of these antennas has also been discussed. The simulation studies reveal that the depicted normalized phase patterns of both the circular waveguide and conical horn follow the changes in the profile of the corresponding amplitude patterns.

1. Introduction

Determination of the near field radiation patterns of antenna elements becomes an important step in the near field beamforming techniques. In open literature, there is an abundance of information on research pertaining to various analytical techniques for the analysis of far field radiation pattern of antennas. The techniques of Method of Moment (MOM), Uniform Geometrical Theory of Diffraction (UGTD), Physical Optics (PO), and Geometrical Optics (GO) are just a few to mention the more commonly and routinely used methods for the determination of far field of antenna. In addition, analytical expressions in closed form are available for certain configurations of antenna elements such as open ended rectangular and circular cylindrical waveguides in [1]. On a relative measure, the literature on techniques for the determination of near field patterns of antennas is rather limited. This can partly be attributed to the spherical wavefront of electromagnetic radiation impinging on the aperture of the antenna under test in the receive mode or the spherical wavefront of the field radiated by the antenna under test in transmit mode. In the past, development of analytical formulation for the near field radiation pattern analysis has been a topic of research and invariably, the emphasis of various research publications is on very specific geometrical configurations of antennas. The near field radiation pattern of conical horn is addressed in [2, 3]. An analysis of near field of point dipoles required for near field array synthesis is given in [4]. The Cartesian components of near field radiation pattern of a point dipole are presented in [5, 6]. From the above succinct citation of various analytical formulations for the analysis of near field radiation pattern of antenna, it is obvious that each of the analytical formulations had been specifically developed keeping the geometric configuration of the antenna and they cannot be extended directly to treat near field analysis of other configurations of antennas implying the lack of generality in the derived analytical formulations. A generalized procedure in the form of a detailed analytical formulation which would facilitate the determination of near field radiation pattern of an antenna of given geometrical configuration including aperture and planar profiles constitutes the primary focus of this paper.

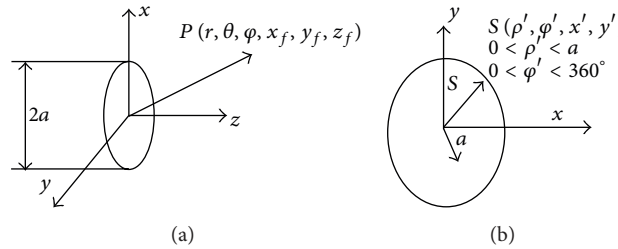

Figure 1: Coordinate system for near field analysis of circular waveguide.

In addition, unlike some of the cited literature above, the proposed near field analysis is valid for the computation of near field radiation pattern in any arbitrarily defined plane of observation leading to the determination of 3D or volumetric radiation pattern which is a requirement in many applications involving antenna engineering [7, 8]. Particularly, for near field beam steering or beamforming scenario covering both azimuthal and elevation angles [7, 8], one needs the near field radiation patterns of antennas in arbitrarily defined planes of observation. The near field beamforming is of potential utility in Through Wall Imaging (TWI) applications. In the proposed analysis, the aperture of the antenna is replaced by an array of point electric and magnetic dipoles. As a consequence, application of this method requires the knowledge of either the current or the field distribution over the radiating aperture of the antenna which for all practical purposes can be obtained with reasonable degree of accuracy and certainty.

2. Generalized Analytical Formulation for Near Field Radiation Pattern of Antenna

This section presents a generalized procedure for the computation of near field radiation pattern of an antenna. The method of determination of near field radiation pattern invokes the concepts of equivalent electric current "J," equivalent magnetic current "M," and the field radiated by the point electric and magnetic dipoles. In the proposed method, the radiating aperture of the antenna is assumed to be replaced by an array of point dipoles (electric/magnetic) whose current strength is determined by the field distribution (magnetic/electric) at the respective locations of dipole. The proposed method is versatile and generic enough to be applicable to any geometric configuration provided that either the field distribution or the current distribution of the antenna is known. For the purpose of illustration, a circular waveguide designed and excited in dominant TE_{11} mode is considered for the analysis.

A conventional circular waveguide with the associated coordinate system for analysis of near field radiation pattern is shown in Figure 1(a). The radiating aperture of the circular waveguide is assumed to coincide with $Z = 0$ plane or XY plane. Observation or field point of interest P is in the near field range of the antenna.

Referring to Figure 1(a), the far field distance criterion for an antenna with aperture of diameter $D = 2a$ is defined as $r \geq 2D^2/\lambda$ where λ is the operating wavelength. The computation or measurement of radiation pattern carried out with point of observation such that $r \leq 2D^2/\lambda$ is usually termed as near field radiation pattern. Reactive field is a specific case of near field with $r < 0.62\sqrt{D^3/\lambda}$. This paper proposes a generalized formulation which is valid to compute radiation patterns of antennas with observation points located in reactive field, near field, and far field of antennas.

The electrical field distribution of the dominant TE_{11} mode of a circular cylindrical wave guide over its aperture is given by [9]

$$E_\rho^{mn\mathrm{TE}}\left(\rho', \phi'\right) = \frac{m}{\rho'} J_m\left(\frac{x'_{mn}}{a}\rho'\right) e^{-jk\rho'} \sin\left(m\phi'\right),$$
$$E_\phi^{mn\mathrm{TE}}\left(\rho', \phi'\right) = \frac{x'_{mn} m}{a} J'_m\left(\frac{x'_{mn}}{a}\rho'\right) e^{-jk\rho'} \cos\left(m\phi'\right). \quad (1)$$

In (1), indices $m = n = 1$ denote the dominant TE_{11} mode of propagation. The radial distance ρ' and angle φ' on the aperture of the waveguide are shown in Figure 1(b). The radius of the circular cylindrical waveguide is denoted by "a." Further $x'_{mn} = 1.841$ for $m = n = 1$. While J_m denotes the cylindrical Bessel function of order m, J'_m refers to the derivative of the Bessel function J_m.

The corresponding aperture magnetic field distribution of the circular waveguide with TE_{11} dominant mode propagation is represented as in [9]

$$H_\rho\left(\rho', \phi'\right) = \frac{E_\rho^{mn\mathrm{TE}}\left(\rho', \phi'\right)}{\omega\mu/K_Z^{\mathrm{TE}}}, \quad (2)$$

$$H_\phi\left(\rho', \phi'\right) = \frac{E_\phi^{mn\mathrm{TE}}\left(\rho', \phi'\right)}{\omega\mu/K_Z^{\mathrm{TE}}}, \quad (3)$$

$$K_Z^{\mathrm{TE}} = \sqrt{k^2 - \left(\frac{x'_{mn}}{a}\right)^2}. \quad (4)$$

With the unit normal of the radiating aperture directed along the z-axis (Figure 1(a)), the equivalent electric "J"

and magnetic "M" currents on the aperture of the circular waveguide are computed from

$$\begin{aligned} J_\rho\left(\rho',\varphi'\right) &= -H_\phi\left(\rho',\varphi'\right), \\ J_\varphi\left(\rho',\varphi'\right) &= H_\rho\left(\rho',\varphi'\right), \\ M_\rho\left(\rho',\varphi'\right) &= E_\phi\left(\rho',\varphi'\right), \\ M_\varphi\left(\rho',\varphi'\right) &= -E_\rho\left(\rho',\varphi'\right). \end{aligned} \tag{5}$$

The Cartesian components of the equivalent currents on the aperture of the waveguide can be written as

$$\begin{aligned} J_x\left(x',y'\right) &= J_\rho\left(\rho',\varphi'\right)\cos\varphi' - J_\phi\left(\rho',\varphi'\right)\sin\varphi', \\ J_y\left(x',y'\right) &= J_\rho\left(\rho',\varphi'\right)\sin\varphi' + J_\phi\left(\rho',\varphi'\right)\cos\varphi', \\ M_x\left(x',y'\right) &= M_\rho\left(\rho',\varphi'\right)\cos\varphi' - M_\phi\left(\rho',\varphi'\right)\sin\varphi', \\ J_y\left(x',y'\right) &= M_\rho\left(\rho',\varphi'\right)\sin\varphi' + M_\phi\left(\rho',\varphi'\right)\cos\varphi'. \end{aligned} \tag{6}$$

In (6), x' and y' denote a point on the aperture of the waveguide (Figure 1(b)). The electric field and magnetic fields radiated by point electric dipole evaluated at an arbitrary field point P are dealt with in [5, 6]. For a point electric dipole with x-directed current (x-directed dipole), the co- and cross polar components of the E- and H-fields at any arbitrary radial distance of observation are given by

$$\begin{aligned} &E_{xx}^{\mathrm{ED}}(x,y,z,r) \\ &= \left\{\frac{\eta}{r^2}\left(2-3\frac{y^2+z^2}{r^2}\right)\right. \\ &\quad \left. - j\left(\frac{\omega u}{r}\left(\frac{y^2+z^2}{r^2}\right)+\frac{\eta}{kr^3}\left(2-3\frac{y^2+z^2}{r^2}\right)\right)\right\}\frac{e^{-jkr}}{4\pi}, \end{aligned} \tag{7}$$

$$E_{yx}^{\mathrm{ED}}(x,y,z,r) = \left\{\frac{3\eta}{r^2}+j\left(\frac{\omega u}{r}-\frac{3\eta}{kr^2}\right)\right\}\frac{yx}{r^2}\frac{e^{-jkr}}{4\pi}, \tag{8}$$

$$E_{zx}^{\mathrm{ED}}(x,y,z,r) = \left\{\frac{3\eta}{r^2}+j\left(\frac{\omega u}{r}-\frac{3\eta}{kr^2}\right)\right\}\frac{zx}{r^2}\frac{e^{-jkr}}{4\pi}, \tag{9}$$

$$H_{xx}^{\mathrm{ED}}(x,y,z,r) = 0, \tag{10}$$

$$H_{yx}^{\mathrm{ED}}(x,y,z,r) = (1+jk)\left(\frac{-z}{r^2}\right)\frac{e^{-jkr}}{4\pi}, \tag{11}$$

$$H_{zx}^{\mathrm{ED}}(x,y,z,r) = (1+jk)\left(\frac{y}{r^2}\right)\frac{e^{-jkr}}{4\pi}, \tag{12}$$

where η = impedance of medium = 120π (free-space),

$$\begin{aligned} x &= x_f - x', \qquad y = y_f - y', \\ z &= z_f - z', \qquad r = \sqrt{x^2+y^2+z^2}, \\ x_f &= r\sin\theta\cos\varphi, \qquad y_f = r\sin\theta\sin\varphi, \\ z_f &= r\cos\theta, \end{aligned} \tag{13}$$

and (x', y', z') and (x_f, y_f, z_f) denote the coordinates of the source point and the observation point, respectively.

In expressions (7) to (12), superscript ED stands for electric dipole. The alphabets in the subscript of expressions (7) to (12) are meant to identify or distinguish between the copolar and cross polar components of the field radiated by the point dipole associated with a designated direction of current. For example, E_{yx}^{ED} denotes the y-component of electric field due the x-directed current in an electric dipole. The concept of duality between J and M, E and H, and H and E, η [10] can be invoked to derive the near fields radiated by magnetic dipole from the knowledge of the fields radiated by corresponding electric dipole. Accordingly, for a point magnetic dipole (MD) with x-directed magnetic current, the fields radiated by x-directed magnetic dipole are given by

$$\begin{aligned} E_{xx}^{\mathrm{MD}}(x,y,z,r) &= 0, \\ E_{yx}^{\mathrm{MD}}(x,y,z,r) &= -(1+jk)\left(\frac{-z}{r^2}\right)\frac{e^{-jkr}}{4\pi}, \\ E_{zx}^{\mathrm{MD}}(x,y,z,r) &= -(1+jk)\left(\frac{y}{r^2}\right)\frac{e^{-jkr}}{4\pi}, \\ &H_{xx}^{\mathrm{MD}}(x,y,z,r) \\ &= \left\{\frac{1}{\eta r^2}\left(2-3\frac{y^2+z^2}{r^2}\right)\right. \\ &\quad \left. - j\left(\frac{\omega u}{r}\left(\frac{y^2+z^2}{r^2}\right)+\frac{1}{\eta k r^3}\left(2-3\frac{y^2+z^2}{r^2}\right)\right)\right\} \\ &\quad \times\frac{e^{-jkr}}{4\pi}, \\ H_{yx}^{\mathrm{MD}}(x,y,z,r) &= \left\{\frac{3}{\eta r^2}+j\left(\frac{\omega u}{r}-\frac{3}{\eta k r^2}\right)\right\}\frac{yx}{r^2}\frac{e^{-jkr}}{4\pi}. \end{aligned} \tag{14}$$

Similarly electric and magnetic fields for y-directed electric dipole are given as follows:

$$\begin{aligned} &E_{yy}^{\mathrm{ED}}(x,y,z,r) \\ &= \left\{\frac{\eta}{r^2}\left(2-3\frac{z^2+x^2}{r^2}\right)\right. \\ &\quad \left. -j\left(\frac{\omega u}{r}\left(\frac{z^2+x^2}{r^2}\right)+\frac{\eta}{kr^3}\left(2-3\frac{z^2+x^2}{r^2}\right)\right)\right\}\frac{e^{-jkr}}{4\pi}, \end{aligned} \tag{15}$$

$$E_{zy}^{\mathrm{ED}}(x,y,z,r) = \left\{\frac{3\eta}{r^2}+j\left(\frac{\omega u}{r}-\frac{3\eta}{kr^2}\right)\right\}\frac{zy}{r^2}\frac{e^{-jkr}}{4\pi}, \tag{16}$$

$$E_{xy}^{\mathrm{ED}}(x,y,z,r) = \left\{\frac{3\eta}{r^2} + j\left(\frac{\omega u}{r} - \frac{3\eta}{kr^2}\right)\right\}\frac{xy}{r^2}\frac{e^{-jkr}}{4\pi}, \quad (17)$$

$$H_{yy}^{\mathrm{ED}}(x,y,z,r) = 0, \quad (18)$$

$$H_{zy}^{\mathrm{ED}}(x,y,z,r) = (1+jk)\left(\frac{-x}{r^2}\right)\frac{e^{-jkr}}{4\pi}, \quad (19)$$

$$H_{xy}^{\mathrm{ED}}(x,y,z,r) = (1+jk)\left(\frac{z}{r^2}\right)\frac{e^{-jkr}}{4\pi}. \quad (20)$$

The electric and magnetic fields radiated by y-directed magnetic dipole are given by

$$E_{yy}^{\mathrm{MD}}(x,y,z,r) = 0,$$

$$E_{zy}^{\mathrm{MD}}(x,y,z,r) = -(1+jk)\left(\frac{-x}{r^2}\right)\frac{e^{-jkr}}{4\pi},$$

$$E_{xy}^{\mathrm{MD}}(x,y,z,r) = -(1+jk)\left(\frac{z}{r^2}\right)\frac{e^{-jkr}}{4\pi},$$

$$H_{yy}^{\mathrm{MD}}(x,y,z,r) = \left\{\frac{1}{\eta r^2}\left(2-3\frac{z^2+x^2}{r^2}\right) - j\left(\frac{\omega u}{r}\left(\frac{z^2+x^2}{r^2}\right) + \frac{1}{\eta k r^3}\left(2-3\frac{z^2+x^2}{r^2}\right)\right)\right\}\frac{e^{-jkr}}{4\pi},$$

$$H_{zy}^{\mathrm{MD}}(x,y,z,r) = \left\{\frac{3}{\eta r^2} + j\left(\frac{\omega u}{r} - \frac{3}{\eta k r^2}\right)\right\}\frac{zy}{r^2}\frac{e^{-jkr}}{4\pi},$$

$$H_{xy}^{\mathrm{MD}}(x,y,z,r) = \left\{\frac{3}{\eta r^2} + j\left(\frac{\omega u}{r} - \frac{3}{\eta k r^2}\right)\right\}\frac{xy}{r^2}\frac{e^{-jkr}}{4\pi}. \quad (21)$$

One of the novelties of the formulation presented in this paper for the computation of radiation patterns of electric and magnetic dipoles is that the equations are valid for both near field and far field observation points. The detailed analysis and the results presented in the Appendix conclusively proves that the derived generic near field equations for radiation patterns of point dipoles reduce (or converge) to conventional far field equations for radiation patterns of point dipoles [11].

For circular waveguide of Figure 1(a), since there is no equivalent electric or magnetic current directed along Z direction, the expressions for field radiated by z-directed electric and magnetic dipoles are not discussed.

At a given observation or field point $P(x_f, y_f, z_f)$, the cartesian components of the electric and magnetic fields due to electric and magnetic dipoles located at a point (x', y', z') on the radiating aperture of the waveguide can be written as

$$E_{xT}(x,y,z,r) = J_x(x',y')E_{xx}^{\mathrm{ED}} + J_y(x',y')E_{xy}^{\mathrm{ED}} + M_x(x',y')E_{xx}^{\mathrm{MD}} + M_y(x',y')E_{xy}^{\mathrm{MD}},$$

$$E_{yT}(x,y,z,r) = J_x(x',y')E_{yx}^{\mathrm{ED}} + J_y(x',y')E_{yy}^{\mathrm{ED}} + M_x(x',y')E_{yx}^{\mathrm{MD}} + M_y(x',y')E_{yy}^{\mathrm{MD}},$$

$$E_{zT}(x,y,z,r) = J_x(x',y')E_{zx}^{\mathrm{ED}} + J_y(x',y')E_{zy}^{\mathrm{ED}} + M_x(x',y')E_{zx}^{\mathrm{MD}} + M_y(x',y')E_{zy}^{\mathrm{MD}},$$

$$H_{xT}(x,y,z,r) = J_x(x',y')H_{xx}^{\mathrm{ED}} + J_y(x',y')H_{xy}^{\mathrm{ED}} + M_x(x',y')H_{xx}^{\mathrm{MD}} + M_y(x',y')H_{xy}^{\mathrm{MD}},$$

$$H_{yT}(x,y,z,r) = J_x(x',y')H_{yx}^{\mathrm{ED}} + J_y(x',y')H_{yy}^{\mathrm{ED}} + M_x(x',y')H_{yx}^{\mathrm{MD}} + M_y(x',y')H_{yy}^{\mathrm{MD}},$$

$$H_{zT}(x,y,z,r) = J_x(x',y')H_{zx}^{\mathrm{ED}} + J_y(x',y')H_{zy}^{\mathrm{ED}} + M_x(x',y')H_{zx}^{\mathrm{MD}} + M_y(x',y')H_{zy}^{\mathrm{MD}}. \quad (22)$$

The Cartesian components of the radiation pattern of the waveguide at a field point $P(r,\theta,\varphi)$ are obtained by integrating (22) over the aperture of the waveguide implying the vector summation of field radiated by the array of electric and magnetic dipoles positioned on the radiating aperture of the waveguide. Consider

$$E_x^{\mathrm{WG}}(r,\theta,\varphi) = \iint_A E_{xT}(x,y,z,r)\,dx'dy',$$

$$E_y^{\mathrm{WG}}(r,\theta,\varphi) = \iint_A E_{yT}(x,y,z,r)\,dx'dy',$$

$$E_z^{\mathrm{WG}}(r,\theta,\varphi) = \iint_A E_{zT}(x,y,z,r)\,dx'dy',$$

$$H_x^{\mathrm{WG}}(r,\theta,\varphi) = \iint_A H_{xT}(x,y,z,r)\,dx'dy',$$

$$H_y^{\mathrm{WG}}(r,\theta,\varphi) = \iint_A H_{yT}(x,y,z,r)\,dx'dy',$$

$$H_z^{\mathrm{WG}}(r,\theta,\varphi) = \iint_A E_{zT}(x,y,z,r)\,dx'dy'. \quad (23)$$

Functional relationships between the positional coordinates of field point $P(r,\theta,\phi,x_f,y_f,z_f)$, the variables (x,y,z), and source points of electric and magnetic dipoles on waveguide aperture $(\rho',\varphi',x',y',z')$ are explicit in (2) and Figure 1(b). The spherical components of the near field radiation pattern of the waveguide at $P(r,\theta,\varphi)$ can now be written as

$$E_\theta^{\mathrm{WG}}(r,\theta,\phi) = E_x^{\mathrm{WG}}\cos\theta\cos\phi + E_y^{\mathrm{WG}}\cos\theta\sin\phi - E_z^{\mathrm{WG}}\sin\theta, \quad (24)$$

$$E_\varphi^{\mathrm{WG}}(r,\theta,\phi) = -E_x^{\mathrm{WG}}\sin\varphi + E_y^{\mathrm{WG}}\cos\varphi, \quad (25)$$

$$H_\theta^{\mathrm{WG}}(r,\theta,\phi) = H_x^{\mathrm{WG}}\cos\theta\cos\phi + H_y^{\mathrm{WG}}\cos\theta\sin\phi - H_z^{\mathrm{WG}}\sin\theta, \quad (26)$$

$$H_\varphi^{\mathrm{WG}}(r,\theta,\phi) = -H_x^{\mathrm{WG}}\sin\varphi + H_y^{\mathrm{WG}}\cos\varphi, \quad (27)$$

where $\phi = 0 - 360^\circ$ and θ is $-180^\circ \le 0^\circ \le +180^\circ$.

It is pertinent to emphasize that the formulation presented in this section is valid to other antenna configurations as well with the corresponding changes in the expressions of electric field distribution and equivalent currents on aperture ((1) and (5)).

3. Simulation Results

This section discusses simulation results of radiation patterns of circular cylindrical waveguide and conical horn obtained through the analysis presented in the earlier section. The results include the surface contour plots of current distribution over radiating aperture and far field and near field radiation patterns of both cylindrical waveguide and conical horn. The discussion in this section also covers the validation studies to substantiate the applicability and appropriateness of the proposed near field analysis of antennas.

3.1. Aperture Current Distribution. The field or current distribution over the aperture of a radiator is a fundamental parameter that determines the radiation characteristics of the antenna. The analysis proposed facilitates considering both the electric current "J" and magnetic current "M" over the radiating aperture. In this section, the simulated surface contour plots of both the electric and magnetic currents over the radiating aperture are discussed. For the simulation, the operating frequency of 9.375 GHz has been chosen for the dominant mode of circular waveguide and conical horn designed for X-band frequencies of 8.2–12.4 GHz. For the simulation of the current distribution over the radiating aperture of circular waveguide, (1) to (3) have been invoked. For the case of conical horn, the aperture field distributions of a conical horn given by [9] are used and they are represented by (28) where L is the axial length of the horn. Consider

$$E_\rho^{mn\mathrm{TE}}(\rho',\phi') = \frac{m}{\rho'}J_m\left(\frac{x'_{mn}}{a}\rho'\right)e^{-jk\sqrt{\rho'^2+L^2}}\sin(m\phi'),$$

$$E_\phi^{mn\mathrm{TE}}(\rho',\phi') = \left(\frac{x'_{mn}}{a}\right)J'_m \times\left(\frac{x'_{mn}}{a}\rho'\right)e^{-jk\sqrt{\rho'^2+L^2}}\cos(m\varphi'). \quad (28)$$

Figure 2 illustrates a geometrical configuration of a conical horn. The radius of aperture "a" for circular waveguide is $a = 1.05$ cm and for the conical horn is 4.1 cm. The semiflare angle is $\alpha_0 = 21.09^\circ$ and the axial length "L" is 10.63 cms. For the generation of source (excitations) points on the aperture, the step size along both the radial (ρ) and azimuthal (φ) directions on the aperture is 36 leading to total number of (36×36) points on the radiating aperture of both the circular waveguide and conical horn. The distributions of the electric "J" and magnetic "M" current on the aperture of the circular waveguide are illustrated in Figure 3 through contour filled images.

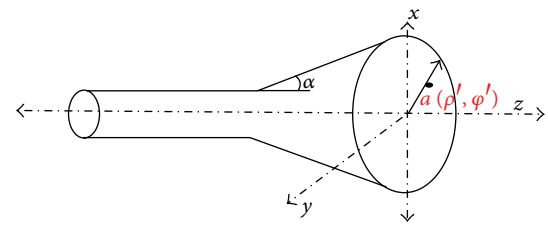

Figure 2: Conical horn antenna.

The corresponding results of conical horn are shown in Figure 4.

3.2. Near Field and Far Field Radiation Patterns. To validate the proposed formulation for the determination of radiation pattern of an antenna at an arbitrary distance covering both the far field and near field, the simulations considered both circular cylindrical waveguide and conical horn as radiating elements.

3.2.1. Circular Cylindrical Waveguide. The validation of the proposed near field radiation was initiated taking the note that the proposed analysis can treat the conventional far field radiation pattern as a special case of near field with the radial distance exceeding or far exceeding the conventional far field criterion. For an X-band circular waveguide radiating at a frequency of 9.375 GHz, $\lambda = 3.2$ cm, the near field distance can be below $2D^2/\lambda$ (<2.55 cm). Using the proposed approach for the determination of near field of an antenna with $r = 1000\lambda$ which clearly falls into far field of an X-band circular waveguide (of radius rad = 1.05 cm) at 9.375 GHz, the far field radiation patterns (E_θ and E_ϕ components) of circular waveguide are computed with the known aperture distribution of the cylindrical waveguide and using (28) as well as the far field analysis given in [12]. The computed results are shown in Figure 5(a). From the results depicted in Figure 5(a), it is evident that the results obtained from the two different formulations show excellent correlation and thereby substantiating the proposed formulation for near field radiation pattern. Figure 5(b) shows another validation for the radiation patterns through far field analysis given in [1]. From the results of Figures 5(a) and 5(b), it is again evident that the results on far field radiation patterns of circular waveguide obtained from the different formulations are in excellent correlation with the proposed formulation for near field radiation pattern. It is pertinent to point out that even though (24) and (25) are specifically meant for the near field radiation patterns of circular waveguides, they are also valid for an observation point located in the far field.

After substantiating the validity of the simulated far field patterns of circular cylindrical waveguide, the computations

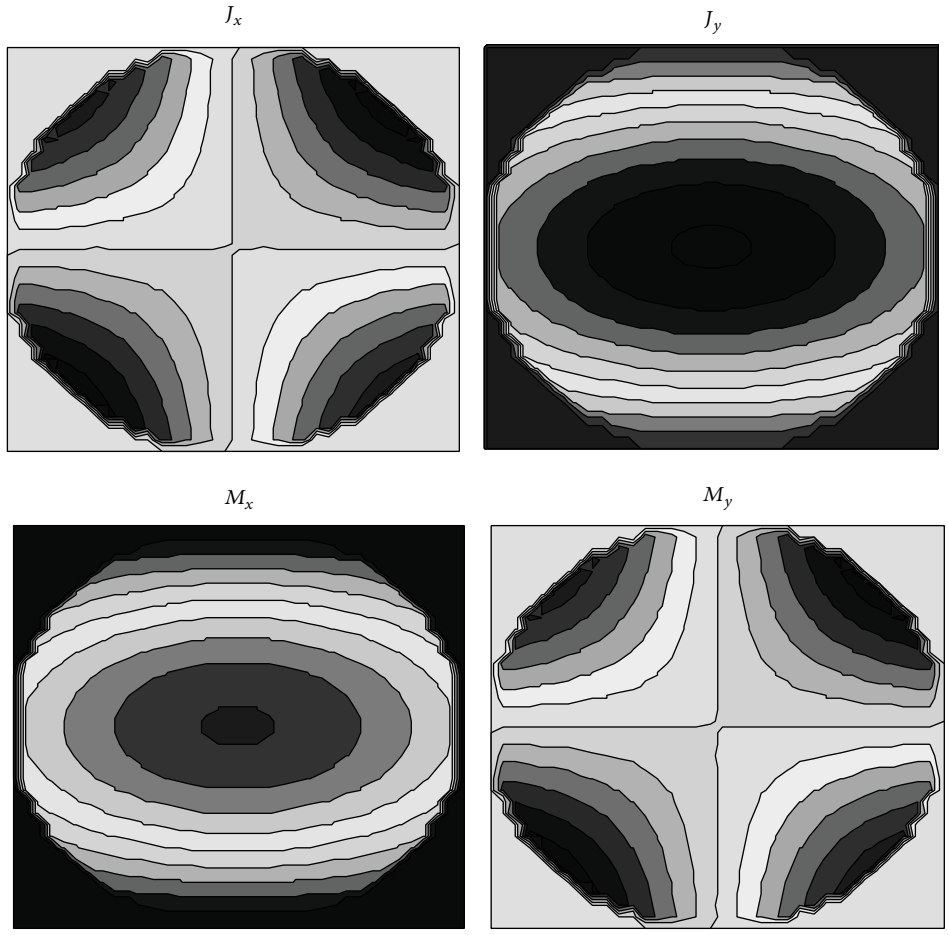

Figure 3: Current distribution over aperture of circular waveguide.

of near field radiation (amplitude and phase) patterns of circular waveguide have been carried out for $r = 0.75\lambda$ at 9.375 GHz and the results are shown in Figures 6(a) and 6(b), respectively.

The radiation patterns of circular waveguide at a radial distance $r = D^2/\lambda$ ($D = 2.1$ cm) and operating at 9.375 GHz are depicted in Figure 7.

An illustration of difference in normalized conventional far field radiation patterns of circular waveguide and the near field radiation pattern at a distance of D^2/λ is shown in Figure 8.

The effect of variation in radial distance on the radiation pattern of circular cylindrical waveguide is shown in Figure 9. Figures 9(a) and 9(b) depict the amplitude of radiation pattern of circular waveguide at $r = D^2/\lambda$ and $r = 2D^2/\lambda$, respectively.

The phase radiation patterns of circular waveguide at $r = D^2/\lambda$ and $r = 2D^2/\lambda$ are shown in Figures 10(a) and 10(b), respectively.

In the analysis of near field radiation pattern, one of the interesting and curious aspects of observation is to monitor the gradual transformation in the profiles of the radiation pattern with the incremental increase in the radial distance of observation. Simulations were carried out to obtain near field patterns of an X-band circular waveguide element at distances of 0.2λ (0.64 cm), 0.3λ (0.96 cm), 0.4λ (1.28 cm), 0.5λ (1.6 cm), and 0.75λ (2.4 cm).

Figure 11 depicts the radiation patterns of a circular waveguide at a distance ($r = 0.2\lambda$ or 0.64 cm) which is relatively very close to the radiating aperture of the waveguide.

A radial distance of $r = 0.2\lambda$ falls within the reactive field region ($r < 0.62\sqrt{D^3/\lambda} = 0.995$ cm) of waveguide. The radiation patterns of the waveguide at this radial distance follow a rather unconventional profile and are drastically different from the conventional far field radiation patterns of an X-band waveguide. The simulation results of the near field radiation patterns of circular waveguide at $r = 0.3\lambda$ (0.96 cm) are shown in Figure 12. The results of Figure 12 reveal that the azimuthal component (E_φ) of the radiation pattern appears to exhibit the main lobe profile although with a reduced gain at the bore sight direction. But the E_θ component of the radiation pattern of the waveguide does not exhibit broadside feature.

When the near field radial distance is increased to $r = 0.4\lambda$, the depicted near field radiation patterns in Figure 13 appear to exhibit the broadside radiating features expected out of circular waveguide.

Both E_φ and E_θ components of the near field radiation pattern shown in Figure 13 exhibit clearly defined

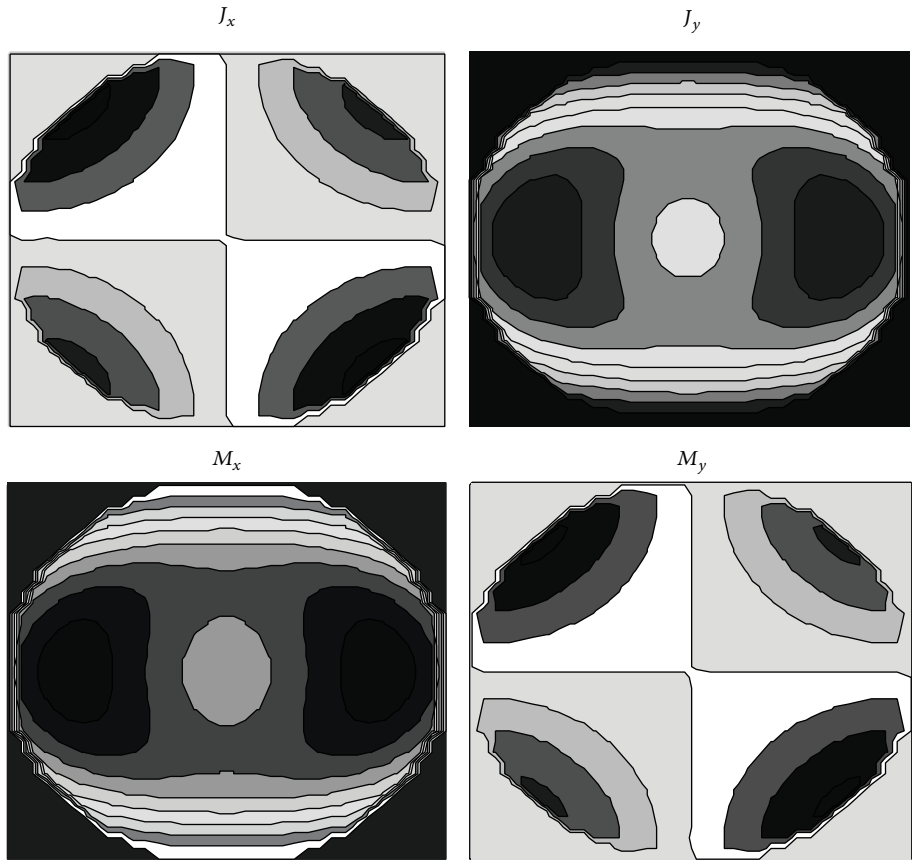

FIGURE 4: Current distribution over aperture of conical horn.

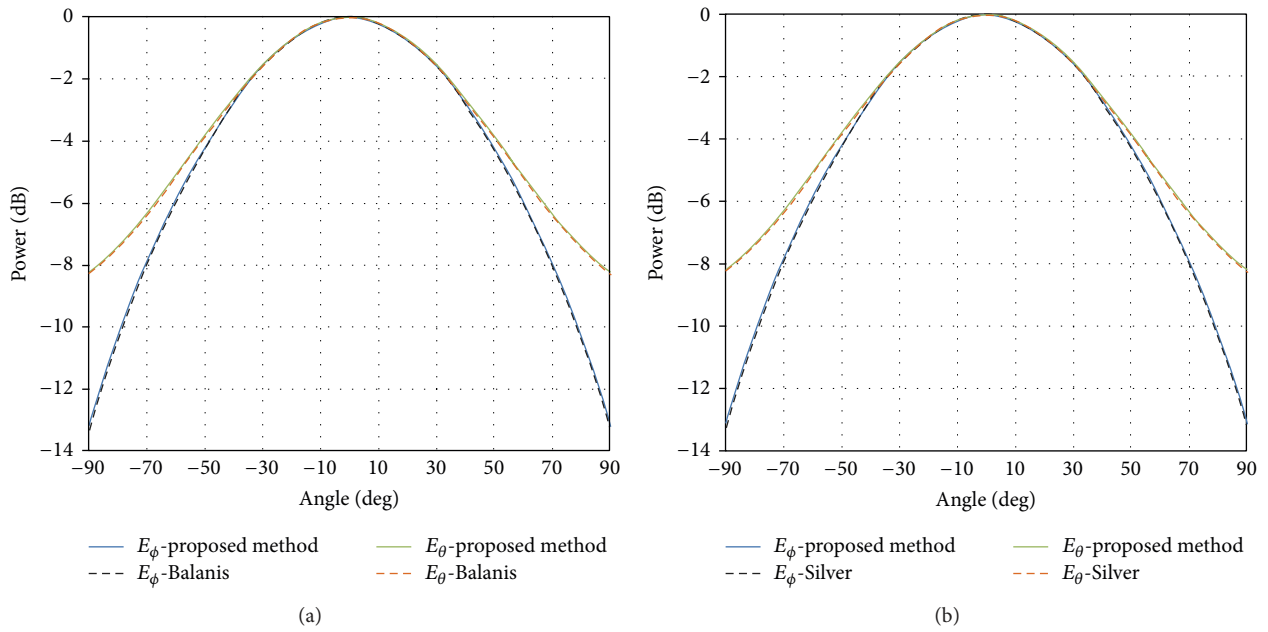

FIGURE 5: (a) Comparison of far field radiation patterns of circular waveguide obtained from [12] and proposed near field method. (b) Comparison of far field radiation patterns of circular waveguide obtained from [1] and proposed near field method.

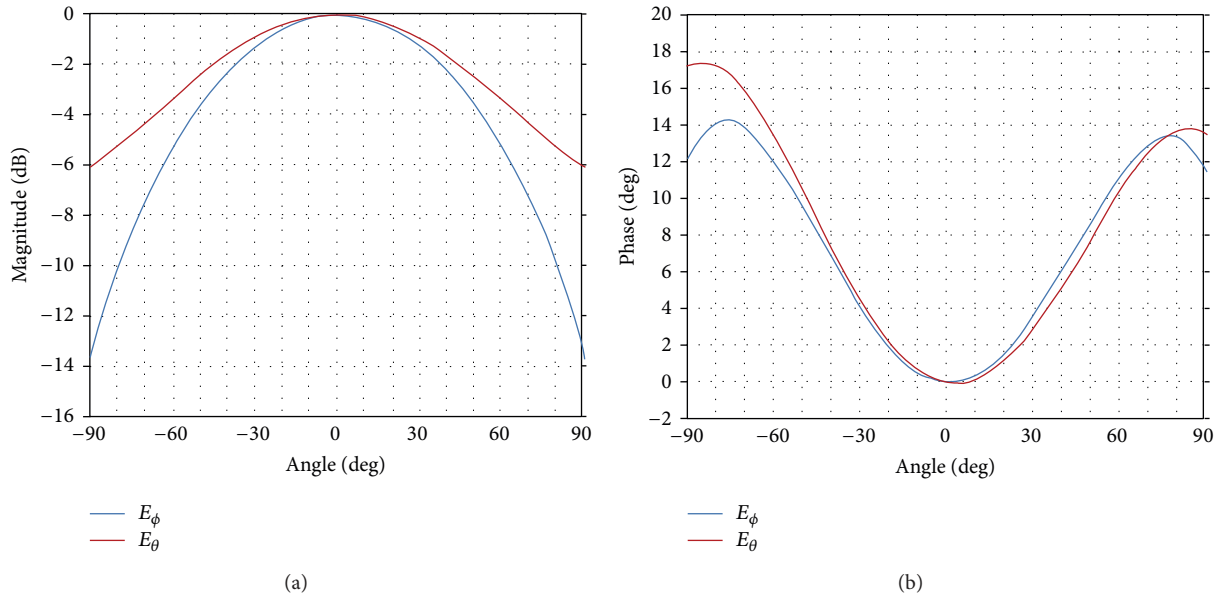

FIGURE 6: (a) Amplitude pattern of a circular waveguide at $r = 0.75\lambda$. (b) Phase pattern of a circular waveguide at $r = 0.75\lambda$.

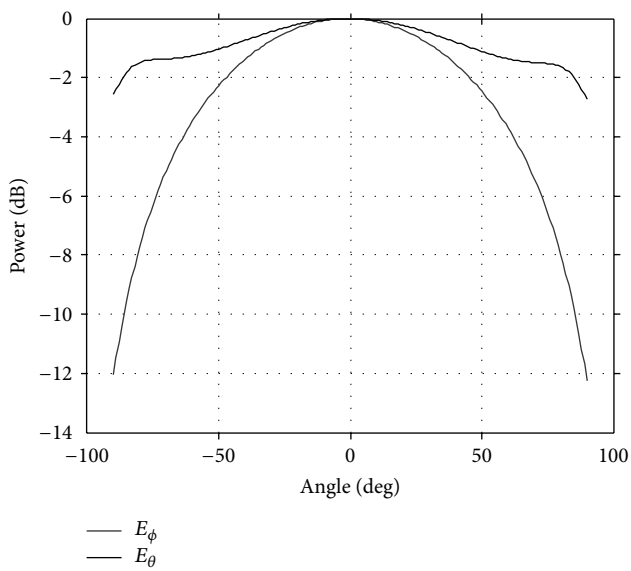

FIGURE 7: Radiation pattern of circular waveguide at a distance of D^2/λ.

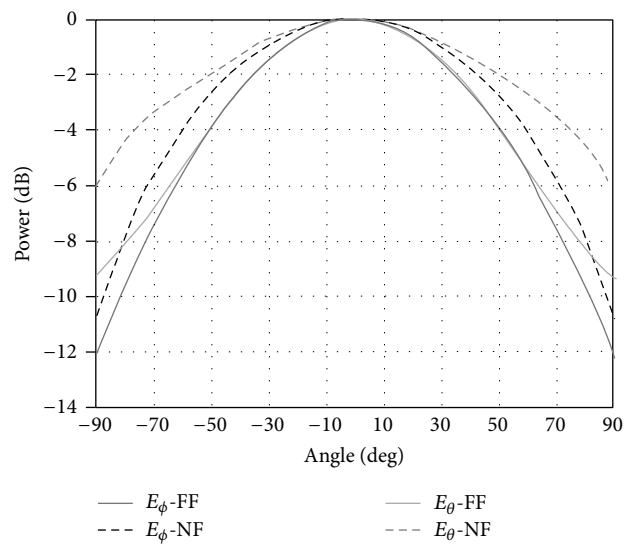

FIGURE 8: Comparison of far field (FF) and near field (NF) pattern of circular waveguide at $r = D^2/\lambda$.

main lobe with E_θ component showing some ripples in the pattern.

At a radial distance of $r = 0.5\lambda$ (1.6 cm), both the components of the radiation pattern exhibit smooth profiles of the main lobe and also the ripples in the E_θ component vanish (Figure 14).

At a distance $r = 0.75\lambda$, the radiation pattern and phase pattern of circular waveguide (Figures 15(a) and 15(b)) show further improvement in the tapering nature of the E_θ component. At $r = 0.75\lambda$, the ratio of radial distance of observation to aperture diameter $(r/D) = 0.571$.

3.2.2. Conical Horn. Conical horn has been one of the most widely radiating elements in antenna engineering. Apart from the far field analysis, the near field analysis of conical horn has also been a topic of research. In the earlier attempts on near field radiation pattern of conical horn, UGTD has been widely invoked [2, 3]. However, the analyses of the two cited research are restricted to the principal planes only. They cannot be applied to arbitrary plane of observation. In this subsection, the simulation results of near field radiation pattern of conical horn derived through the proposed generalized near field analysis are presented. Unlike the above cited prior research on the near field pattern of conical horn,

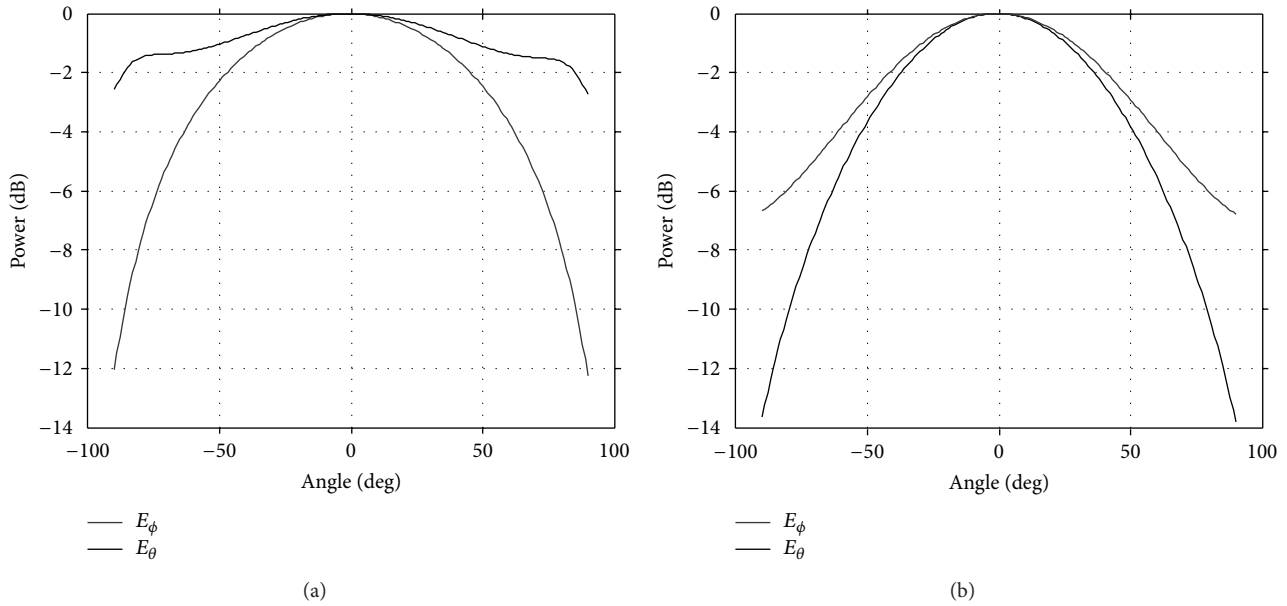

FIGURE 9: Amplitude radiation patterns of circular waveguide. (a) $r = D^2/\lambda$; (b) $r = 2D^2/\lambda$.

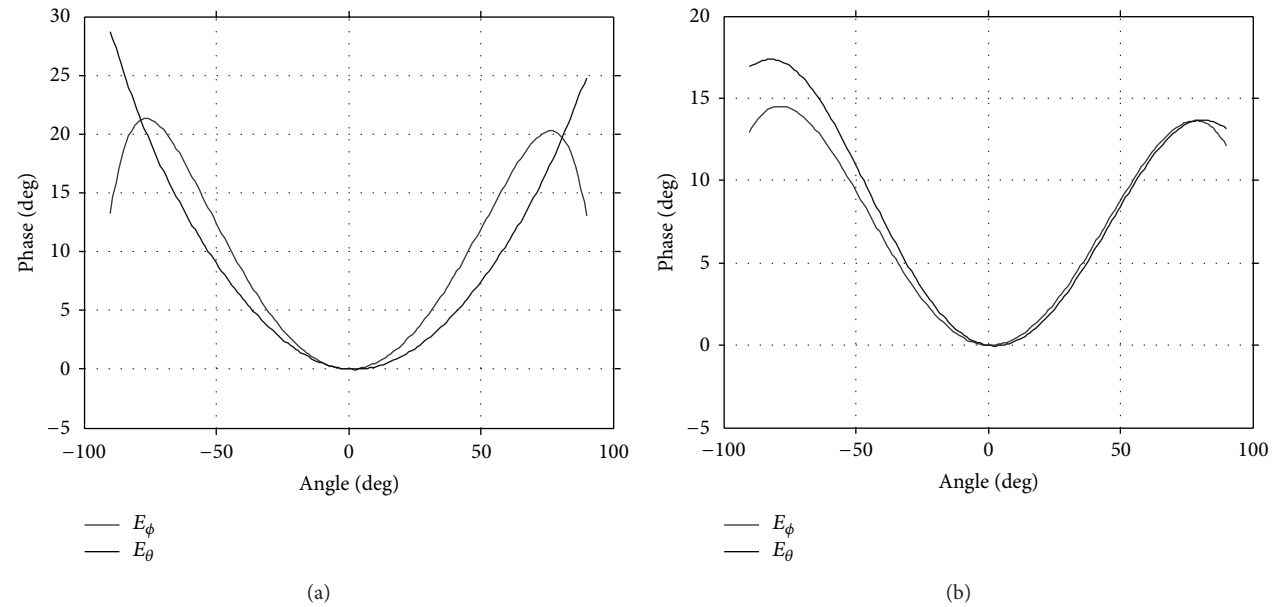

FIGURE 10: (a) Phase radiation pattern of circular waveguide at $r = D^2/\lambda$. (b) Phase radiation pattern of circular waveguide at $r = 2D^2/\lambda$.

the analysis proposed in this paper facilitates the near field computation of conical horn in any arbitrary plane in 3D space which is required in beam steering scenario covering both azimuthal and elevation angles. From the analytical formulation point of view, the circular cylindrical waveguide configuration can be considered as a limiting case of a conical horn of semiflare angle of zero degrees.

The coordinate system for near field radiation pattern analysis of a conical horn is shown in Figure 2. The analysis for the determination of near field radiation pattern of circular cylindrical waveguide is extended to the case of conical horn without loss of generality. All the equations developed for the near field radiation pattern analysis of circular waveguide are identically valid to conical horn. The distribution of electric field over the radiating aperture of conical horn is given by (28).

As an initial step, the radiation patterns of conical horn with semiflare angle $\alpha_0 = 21.09^\circ$ and radius = 4.1 cm operating at 9.375 GHz are simulated at radial distance $r = 1000\lambda$. At this radial distance, the simulation meets and far exceeds the conventional far field distance criterion. In addition, the formulation available in [12] which is valid only for the far

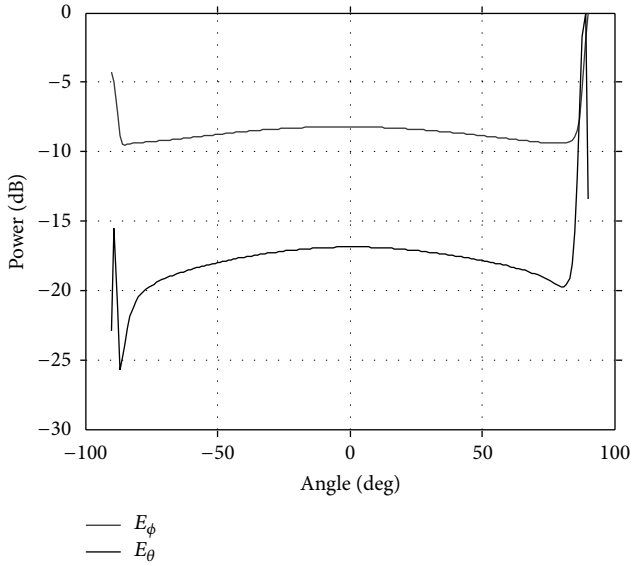

Figure 11: Near field radiation pattern of circular waveguide at $r = 0.2\lambda$ (0.64 cm).

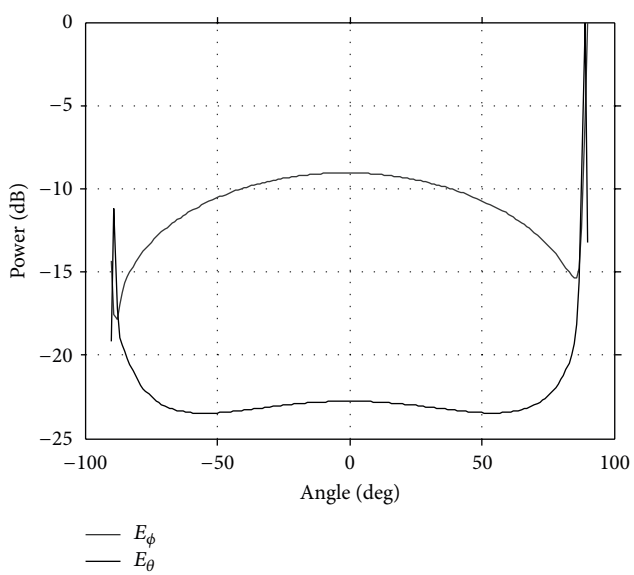

Figure 12: Radiation pattern of circular waveguide at $r = 0.3\lambda$ (0.96 cm).

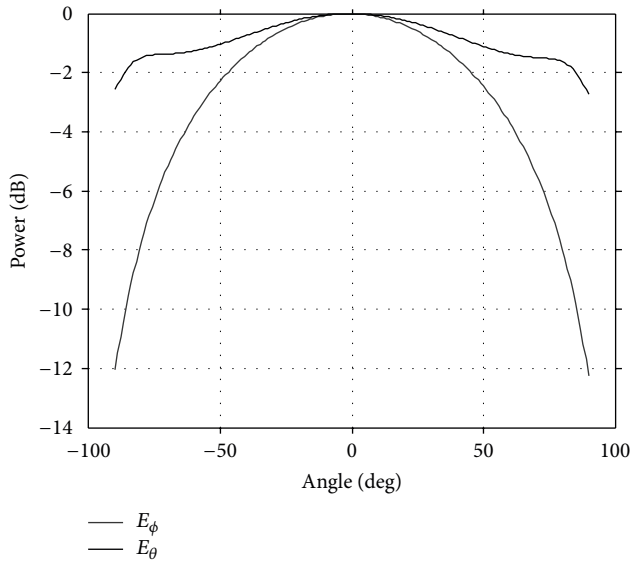

Figure 13: Radiation pattern of circular waveguide at $r = 0.4\lambda$ (1.28 cm).

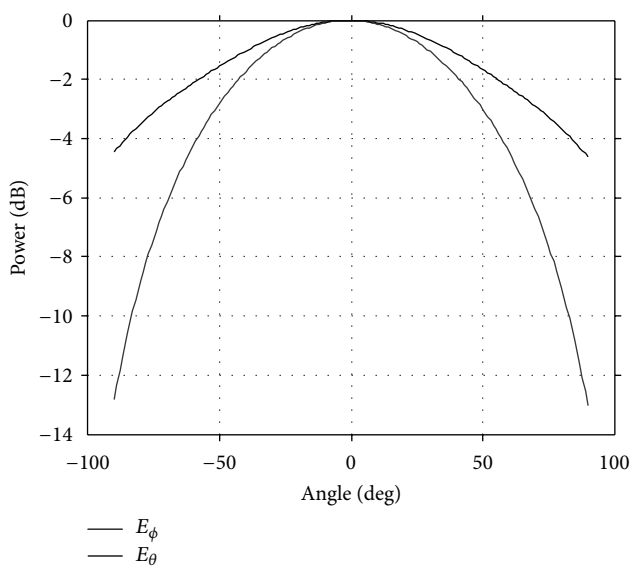

Figure 14: Radiation pattern of circular waveguide at $r = 0.5\lambda$ (1.6 cm).

field radiation patterns is also made use of to obtain the far field radiation patterns of conical horn. The results derived through the formulation in [12] serve as a reference to validate the results obtained through the proposed formulation for the determination of radiation pattern of antenna at any arbitrary distance. The results depicted in Figure 16 clearly illustrate the excellent correlation between the results obtained through the analysis of [12] and the new near field formulation proposed in this paper. For the simulations, conical horn of radius = 4.1 cm and semiflare angle $\alpha_0 = 21.09^\circ$ was considered with an operating frequency at 9.375 GHz.

It is pertinent to point out that the analytical formulation proposed in this paper is valid for any arbitrary distance of observation implying that it is applicable equally well for both near field and far field radiation pattern. The near field radiation patterns of conical horn of semiflare angle $\alpha_0 = 21.09^\circ$ and radius = 4.1 cm at a radial distance of D^2/λ operating at 9.375 GHz are shown in Figure 17.

A comparison of radiation patterns of conical horn (semiflare angle $\alpha_0 = 21.09^\circ$) is evaluated at radial distances of $r = D^2/\lambda$ and their far field radiation patterns are illustrated in Figure 18.

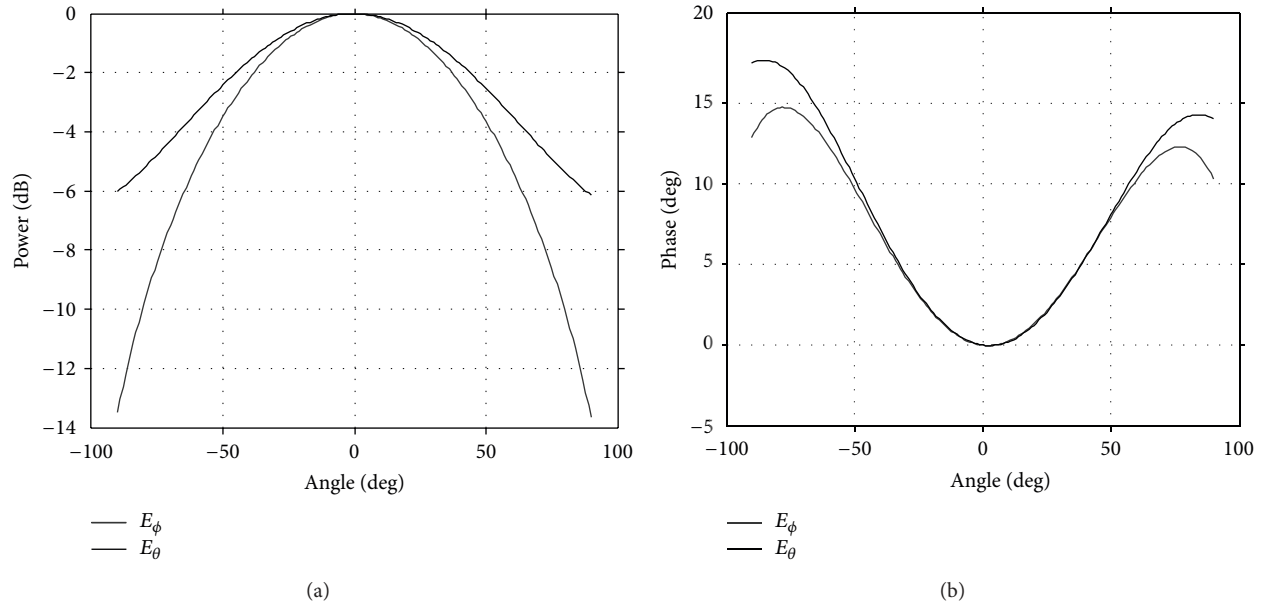

FIGURE 15: (a) Radiation pattern of circular waveguide at a distance $r = 0.75\lambda$. (b) Phase pattern of circular waveguide at a distance $r = 0.75\lambda$.

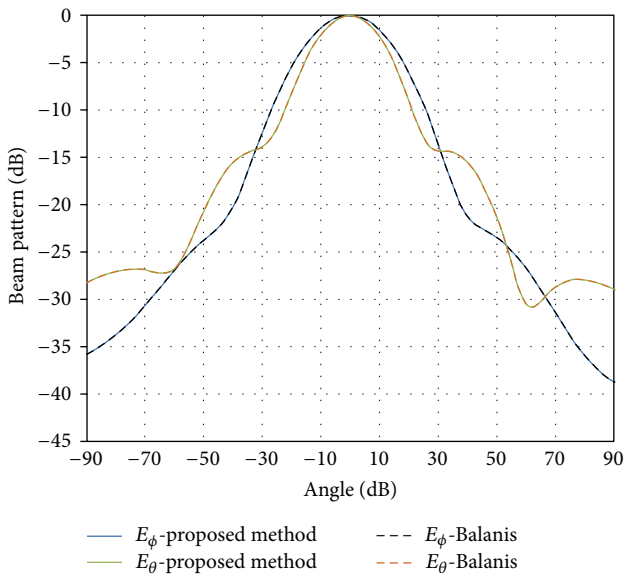

FIGURE 16: Comparison of far field radiation patterns of conical horn antenna obtained from [x] and proposed near field method.

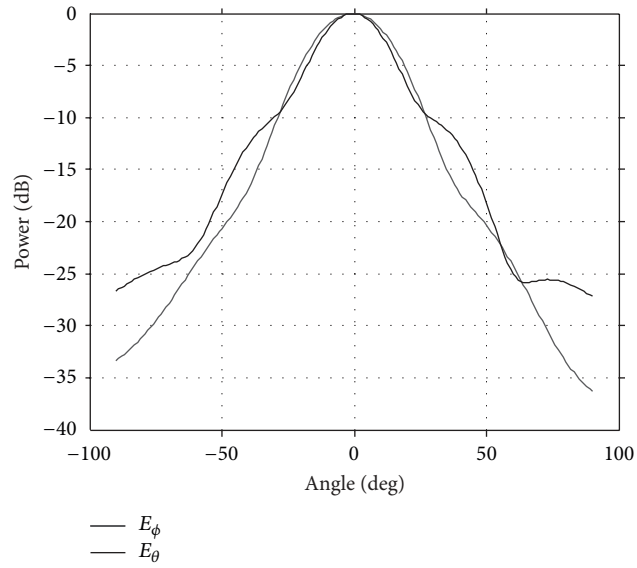

FIGURE 17: Near field radiation pattern of conical horn at $r = D^2/\lambda$.

The effect of variation in radial distance of observation on the radiation pattern of conical horn is illustrated in Figures 19 and 20. The near field radiation patterns of conical horn at a radial distance of $r = D^2/\lambda$ are shown in Figure 19(a). The corresponding radiation patterns at $r = 2D^2/\lambda$ are depicted in Figure 19(b).

The results of Figures 20(a) and 20(b) illustrate the phase radiation patterns of the conical horn at radial distances of $r = D^2/\lambda$ and $2D^2/\lambda$, respectively.

On comparing near field and far field magnitude and phase plots of Figures 19 and 20, a clear indication in change of phase and beam widths can be noticed when the radial distance of observation is varied.

The analysis of near field radiation pattern was carried out for conical horn antenna to observe the gradual transformation in the profiles of the radiation pattern with the incremental increase in the radial distance of observation. Simulations were carried out to obtain near field patterns of an X-band conical horn antenna at radial distances of 1λ, 2λ, 3λ, 4λ, and 10λ.

For a conical horn antenna operating at 9.375 GHz with a radius of 4.1 cm, a radial distance of $r = 1\lambda$ falls within the reactive field region ($r < 0.62\sqrt{D^3/\lambda} = 8.1$ cm).

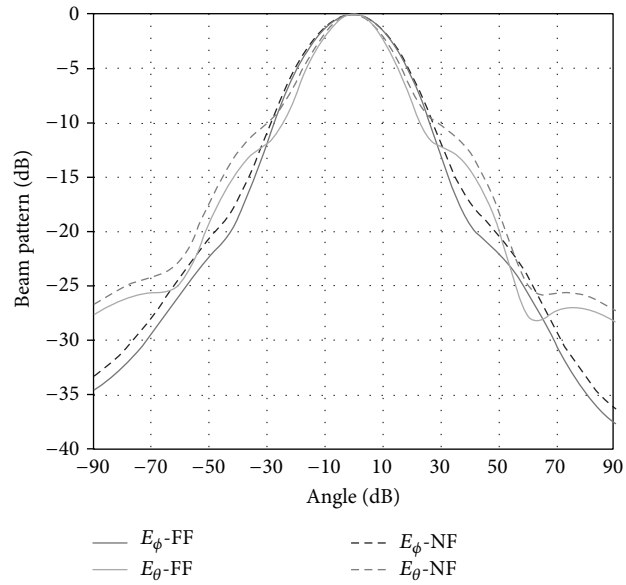

Figure 18: Comparison of near field and far field radiation patterns of conical horn (radius = 4.1 cm; semiflare angle $\alpha_0 = 21.09^\circ$).

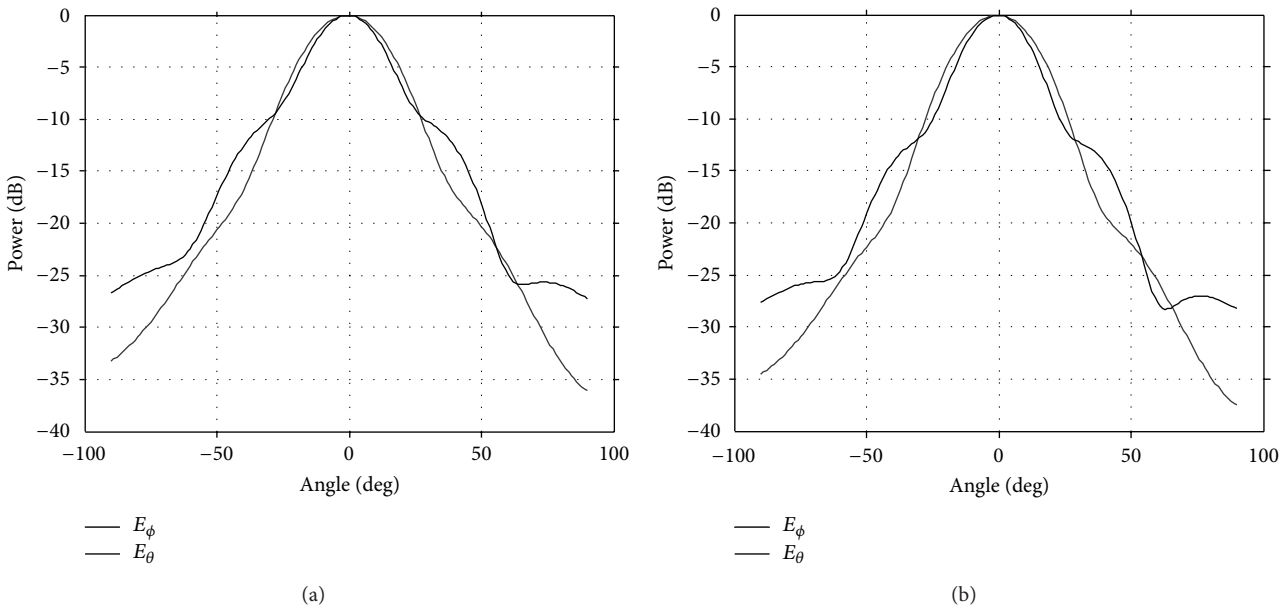

Figure 19: Comparison of amplitude radiation pattern of conical horn: (a) $r = D^2/\lambda$, (b) $r = 2D^2/\lambda$.

The simulation results of the near field amplitude and phase radiation patterns of the conical horn with semiflare angle $\alpha_0 = 21.09^\circ$ and radius = 4.1 cm at $r = 1\lambda$ are shown in Figures 21(a) and 21(b). The radiation patterns of the conical horn antenna at this radial distance are drastically different from its conventional far field radiation patterns. The results of Figure 21 reveal that both the azimuthal (E_φ) and elevation (E_θ) components of the radiation patterns do not exhibit broadside feature of a conical horn.

When the near field radial distance is increased to $r = 2\lambda$, the near field radiation patterns appear to exhibit the broadside radiating features expected out of conical horn antenna. Both the E_φ and E_θ components of the near field amplitude and phase radiation patterns shown in Figures 22(a) and 22(b) exhibit clearly defined main lobe with E_θ component showing some ripples in its pattern. At $r = 2\lambda$, the ratio of radial distance of measurement to diameter of radiating aperture $(r/D) = 0.781$.

At a radial distance of $r = 3\lambda$, both the components of the radiation pattern exhibit smooth profiles of the main lobe and also the ripples in the E_θ component vanish (Figure 23).

At a distance $r = 10\lambda$, the amplitude and phase patterns of conical horn (Figure 24) show further improvement in the drooping (tapering) nature in the E_θ component.

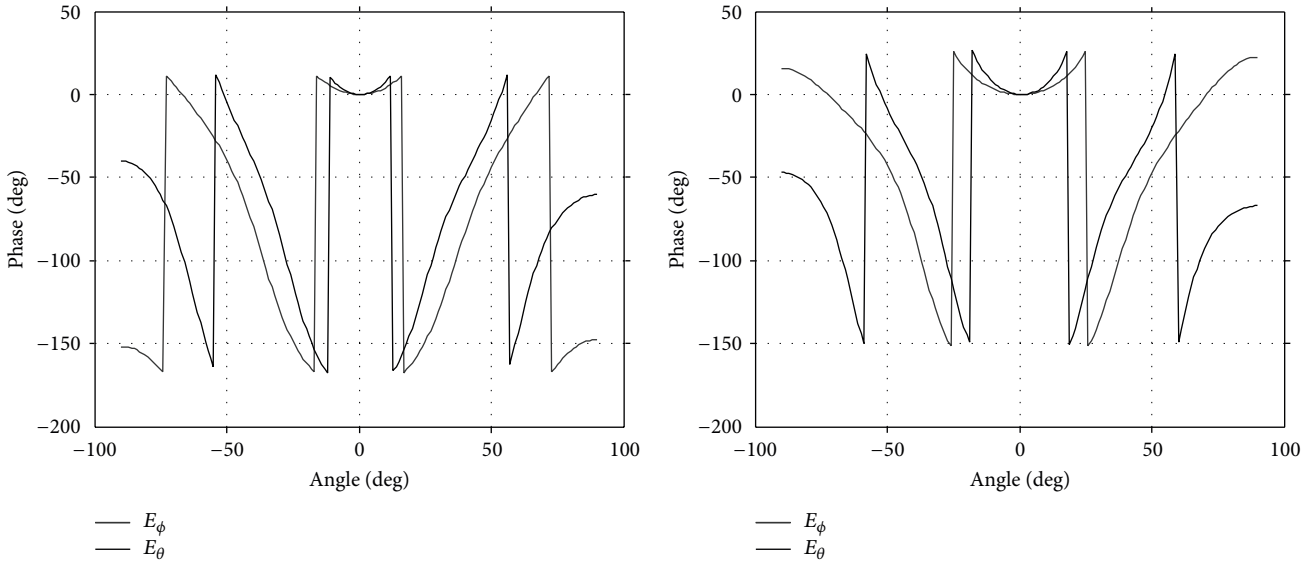

FIGURE 20: Comparison of phase radiation pattern of conical horn: (a) $r = D^2/\lambda$, (b) $r = 2D^2/\lambda$.

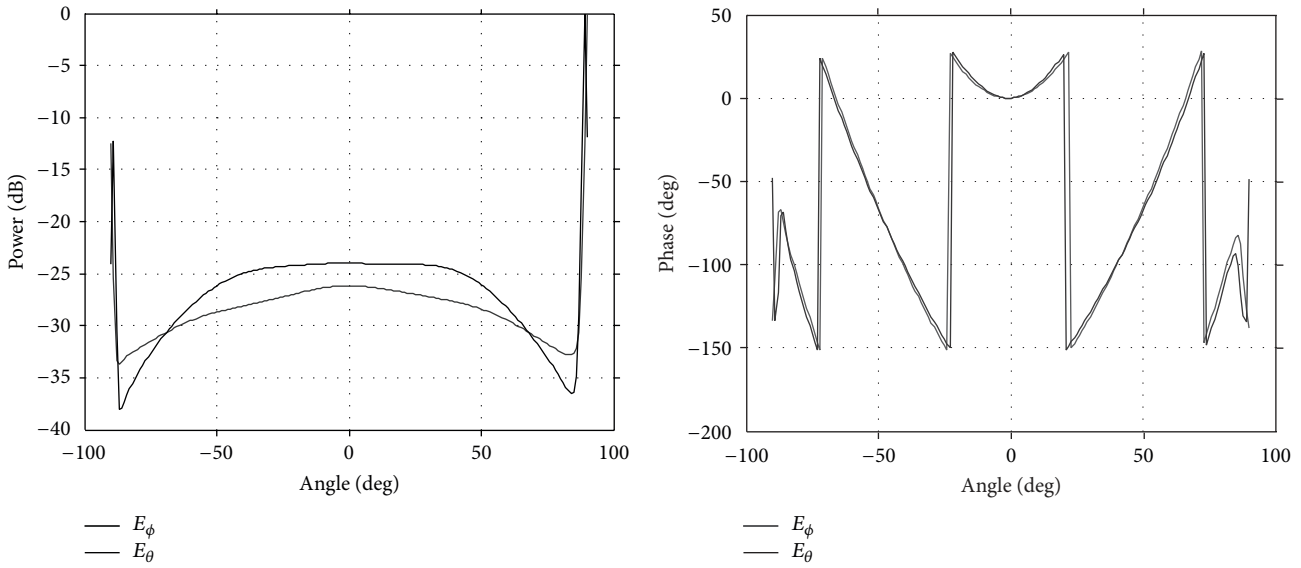

FIGURE 21: (a) Near field radiation pattern of conical horn at a distance $r = 1\lambda$ (3.2 cm). (b) Near field phase pattern of conical horn at a distance $r = 1\lambda$ (3.2 cm).

For a conical horn with a radius of aperture of 4.1 cm operating at 9.375 GHz, the radial distance of measurement of $r = 10\lambda$ still corresponds to near field distance of observation.

4. Conclusion

This section summarizes the conclusions that can be derived out of the analysis and simulation results presented in this paper.

A generalized procedure in the form of an analytical formulation for the determination of radiation pattern of an antenna at any arbitrary distance which covers the near field as well as far field is presented in this paper. With the prior knowledge of either the current or field distribution on the radiating aperture, the proposed near field analysis is generic and can be applied for wide variety of antenna elements. The underlying principle of the generalized procedure is tantamount to considering the radiating aperture as an array of point electric and magnetic dipoles. The radiation pattern of the antenna at any arbitrary point of observation (valid for both near field and far field) is obtained by the vector summation of the fields radiated by the array of both electric and magnetic dipoles located on the aperture of the antenna.

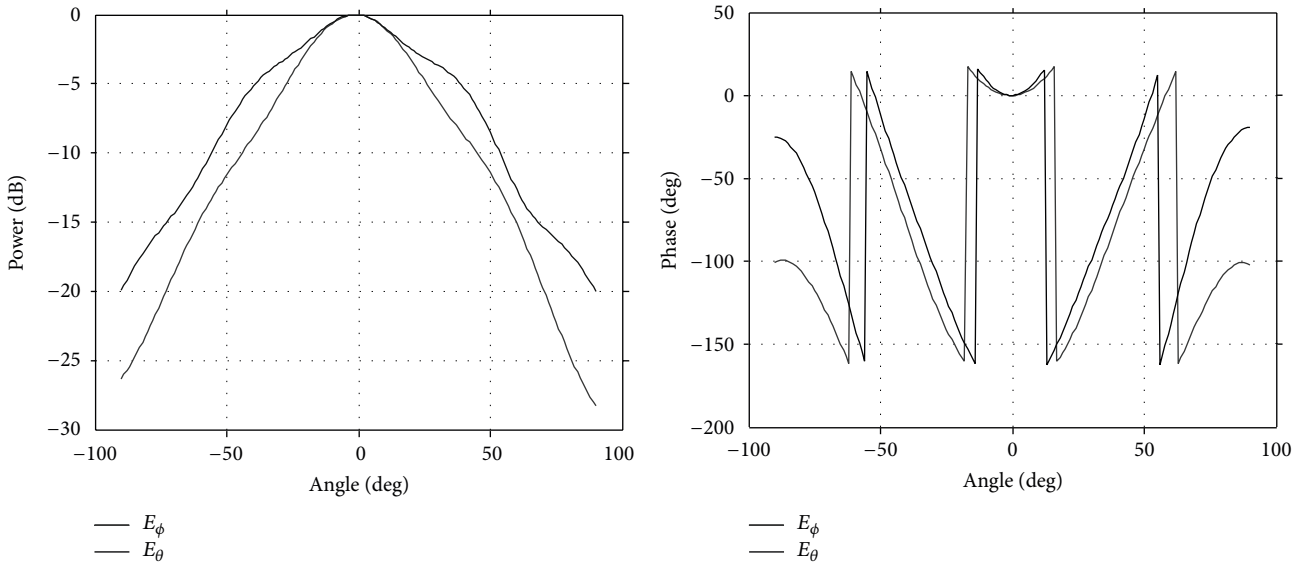

(a) (b)

Figure 22: Near field radiation pattern of conical horn at $r = 2\lambda$ (6.4 cm).

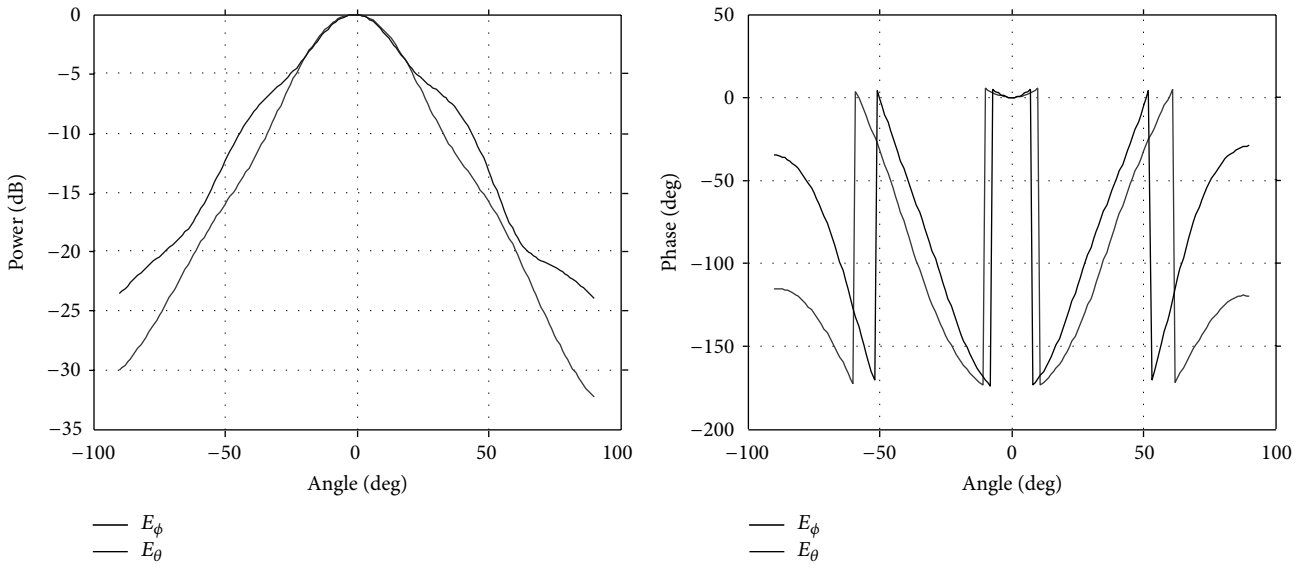

(a) (b)

Figure 23: (a) Near field radiation pattern of conical horn at a distance $r = 3\lambda$ (9.6 cm). (b) Near field phase pattern of conical horn at a distance $r = 3\lambda$ (9.6 cm).

The significance of the proposed analysis lies in the derivation of explicit expressions for the copolar and cross polar components of the radiation pattern of both electric and magnetic dipoles. In addition, in the analysis both the Cartesian and spherical polar components of the near field radiation patterns are emphasized. The spherical polar representation is of direct relevance to conventional antenna engineering analysis of individual radiators and beam forming analysis. The Cartesian representation of the proposed near field analysis is tailor made for initial computations in TWI. With the circular cylindrical waveguide and conical horn as radiating elements, this paper has established and substantiated the generic and versatile features of proposed novel approach for the determination of near field radiation pattern of these antennas.

To take advantage of the available results through the well-established analytical formulations which are valid exclusively for the far field radiation patterns of antennas, initial simulations of the proposed near field analysis have been carried out with radial distance of observation satisfying the criterion of far field. The simulation results of the proposed near field analysis with the radial distance of observation of 1000λ show excellent correlation with the results derived through analytical formulations

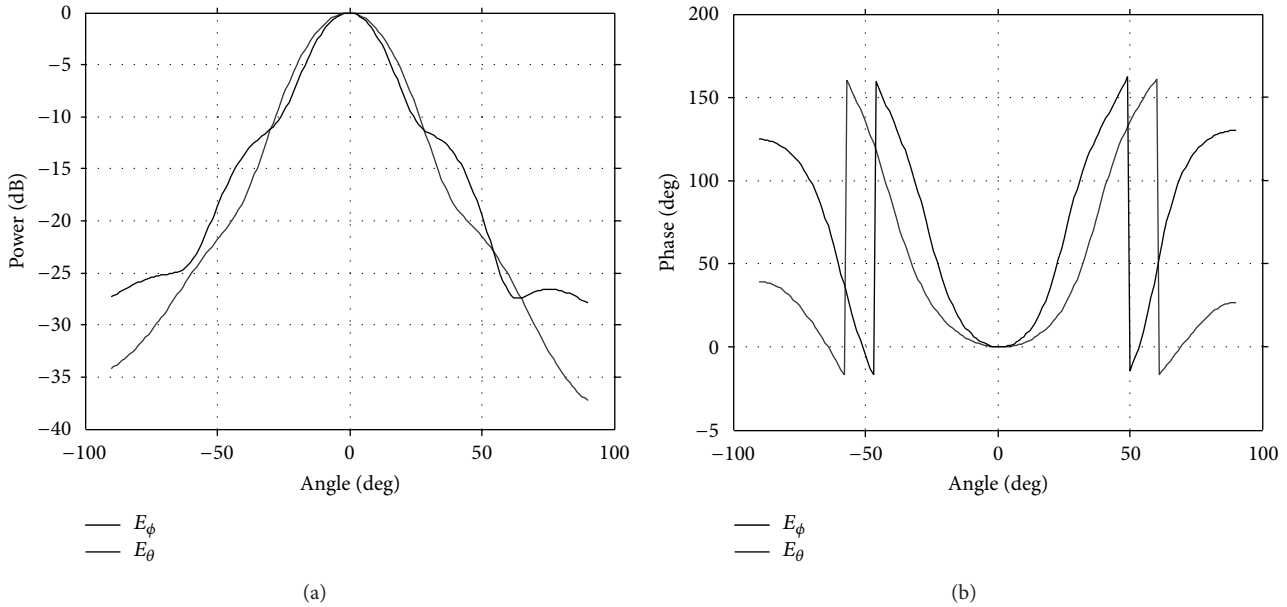

Figure 24: (a) Radiation pattern of conical horn at $r = 10\lambda$ (32 cm). (b) Phase pattern of conical horn at $r = 10\lambda$ (32 cm).

of [1, 12] which are exclusively valid only for the far field.

After substantiating the validity of the proposed analysis for the special case of far field, numerous simulations have been performed to study and analyze the radiation patterns of circular waveguide and conical horn at radial distances of observation lying very close to the radiating aperture.

At a distance of 0.2λ from the aperture, the radiation patterns of circular waveguide are vastly/drastically different from the corresponding conventional far field patterns. The broadside radiating feature of the circular waveguide is also absent. As is expected, with the gradual increase in the radial distance of observation, one notices the increasing trend in the radiation patterns of circular waveguides to broadly conform to the profile of conventional far field patterns. The radiation patterns nearly resemble the corresponding conventional far field patterns at $r = 0.75\lambda$ for circular waveguide and correspond to $(r/D) = 0.571$. For a conical horn with a radius of 4.1 cm, the radiation patterns at $r = 2\lambda$ show defined main lobe and $r = 2\lambda$ is equivalent to $(r/D) = 0.781$.

The depicted normalized phase patterns of both the circular waveguide and conical horn follow the changes in the profile of the corresponding amplitude patterns.

The successful formulation and validation of the approach for the determination of near field radiation pattern of an antenna presented in this paper is an important step to progress to the next significant analytical formulations involving a new approach for near field beamforming technique which is the research topic of interest of the authors.

Appendix

The primary emphasis of this appendix is to establish that the derived equations for near field radiation patterns of electric and magnetic dipoles get simplified when observation point moves to far field and the simplified equations are identical to the available standard equations far field radiation patterns of dipole [11, page 155]. In addition, this appendix demonstrates that the generic formulations of this paper when extended to far field computations yield the same results as that derived through conventional far field equations of point dipoles. This appendix also presents far field equations (for both co- and cross polar components) of radiation patterns of electric point dipoles. The concept of duality can then be extended to derive the corresponding equations of magnetic dipole.

The generalized equations for far field radiation patterns of a x-directed electric point dipole given in [11, page 155] are

$$E_\theta^x(r,\theta,\varphi) = -\frac{j\omega\mu Il}{4\pi r}(\cos\theta\cos\varphi)\,e^{-jkr},$$
$$E_\varphi^x(r,\theta,\varphi) = -\frac{j\omega\mu Il}{4\pi r}(\sin\varphi)\,e^{-jkr}. \tag{A.1}$$

The corresponding x component of the far field radiation pattern of x-directed electric point dipole can be determined through

$$E_x(r,\theta,\varphi) = E_\theta\cos\theta\cos\varphi - E_\varphi\sin\varphi. \tag{A.2}$$

Substituting (A.1) in (A.2), the x component of the far field radiation pattern of a x-directed electric point dipole simplifies to

$$E_x(r,\theta,\varphi) = -\frac{j\omega\mu Il}{4\pi r}e^{-jkr}\left(\cos^2\theta + \sin^2\varphi\sin^2\theta\right). \tag{A.3}$$

Analogous far field radiation patterns of a y-directed electric point dipole [11] are

$$E_\theta^y(r,\theta,\varphi) = -\frac{j\omega\mu Il}{4\pi r}(\cos\theta\sin\varphi)\,e^{-jkr},$$
$$E_\varphi^y(r,\theta,\varphi) = -\frac{j\omega\mu Il}{4\pi r}(\cos\varphi)\,e^{-jkr}. \tag{A.4}$$

The y component of the far field component of a y-directed electric dipole can be written as

$$E_y = E_\theta \cos\theta \sin\varphi - E_\varphi \cos\varphi. \quad (A.5)$$

Upon substitution of (A.4) into (A.5) and further simplification, the y-directed component of far field radiation pattern of y-directed electric point dipole is determined through

$$E_y(r,\theta,\varphi) = -\frac{j\omega\mu Il}{4\pi r} e^{-jkr}\left(\cos^2\theta + \cos^2\varphi \sin^2\theta\right). \quad (A.6)$$

Similarly the far field radiation pattern of z-directed electric point dipole given in [11] is

$$E_\theta^z(r,\theta,\varphi) = -\frac{j\omega\mu Il}{4\pi r}(\sin\theta)\, e^{-jkr}. \quad (A.7)$$

The z-component of the far field radiation pattern of z-directed electric point dipole can then be written as

$$E_z = E_\theta \sin\theta. \quad (A.8)$$

On substitution of (A.8) and by simplification, (A.8) can further be written as

$$E_Z(r,\theta,\varphi) = -\frac{j\omega\mu Il}{4\pi r}\sin^2\theta e^{-jkr}. \quad (A.9)$$

Equations (A.3), (A.6), and (A.9) are the Cartesian far field copolar components of x-directed, y-directed, and z-directed electric point dipoles, respectively.

For the computations of far field radiation patterns, the expressions for copolar components of near field radiation patterns of $E_{xx}^{\mathrm{ED}}()$ x-directed, $E_{yy}^{\mathrm{ED}}()$ y-directed electric point dipoles given in (7) and (15) can be simplified to a more compact form to retain the field variation of the form e^{-jkr}/r in the far field. Consider

$$E_{xx}^{\mathrm{ED}}(x,y,z,r) = \left\{-j\left(\frac{\omega u}{r}\left(\frac{y^2+z^2}{r^2}\right)\right)\right\}\frac{e^{-jkr}}{4\pi}, \quad (A.10)$$

$$E_{yy}^{\mathrm{ED}}(x,y,z,r) = \left\{-j\left(\frac{\omega u}{r}\left(\frac{x^2+z^2}{r^2}\right)\right)\right\}\frac{e^{-jkr}}{4\pi}. \quad (A.11)$$

Similarly, copolar component of the far field radiation pattern of a z-directed electric point dipole is given by

$$E_{zz}^{\mathrm{ED}}(x,y,z,r) = \left\{-j\left(\frac{\omega u}{r}\left(\frac{x^2+y^2}{r^2}\right)\right)\right\}\frac{e^{-jkr}}{4\pi}, \quad (A.12)$$

where

$$x = x_f - x_s, \qquad y = y_f - y_s, \qquad z = z_f - z_s. \quad (A.13)$$

For a point dipole located at the origin, $x_s = y_s = z_s = 0$. Also, the Cartesian coordinates of observation points are written as

$$x_f = r\sin\theta\cos\varphi, \qquad y_f = r\sin\theta\sin\varphi, \qquad z_f = r\cos\theta, \quad (A.14)$$

where r is the far field distance of observation from the origin.

Substituting (A.13)-(A.14) in (A.10)–(A.12)

$$E_{xx}^{\mathrm{ED}}(x,y,z,r) = \left\{-j\left(\frac{\omega u}{r}\left(\frac{y^2+z^2}{r^2}\right)\right)\right\}\frac{e^{-jkr}}{4\pi}, \quad (A.15)$$

$$E_{xx}^{\mathrm{ED}}(r,\theta,\varphi) = \left\{-j\left(\frac{\omega u}{r}\left(\frac{(r\sin\theta\ \sin\varphi)^2 + (r\cos\theta)^2}{r^2}\right)\right)\right\}\frac{e^{-jkr}}{4\pi}, \quad (A.16)$$

$$E_{xx}^{\mathrm{ED}}(r,\theta,\varphi) = -j\frac{\omega u}{r}\frac{e^{-jkr}}{4\pi r}\left(\frac{\left(\sin^2\theta\sin^2\varphi\right) + \left(\cos^2\theta\right)}{r^2}\right), \quad (A.17)$$

$$E_{yy}^{\mathrm{ED}}(x,y,z,r) = \left\{-j\left(\frac{\omega u}{r}\left(\frac{x^2+z^2}{r^2}\right)\right)\right\}\frac{e^{-jkr}}{4\pi}, \quad (A.18)$$

$$E_{yy}^{\mathrm{ED}}(r,\theta,\varphi) = \left\{-j\left(\frac{\omega u}{r}\left(\frac{\left(\sin^2\theta\cos^2\varphi\right) + \left(\cos^2\theta\right)}{r^2}\right)\right)\right\} \times \frac{e^{-jkr}}{4\pi}, \quad (A.19)$$

$$E_{yy}^{\mathrm{ED}}(r,\theta,\varphi) = -j\frac{\omega u}{r}\frac{e^{-jkr}}{4\pi r}\left(\frac{\sin^2\theta\cos^2\varphi + \left(\cos^2\theta\right)}{r^2}\right), \quad (A.20)$$

$$E_{zz}^{\mathrm{ED}}(x,y,z,r) = \left\{-j\left(\frac{\omega u}{r}\left(\frac{x^2+y^2}{r^2}\right)\right)\right\}\frac{e^{-jkr}}{4\pi}, \quad (A.21)$$

$$E_{zz}^{\mathrm{ED}}(r,\theta,\varphi) = \left\{-j\left(\frac{\omega u}{r}\left(\frac{\left(\sin^2\theta\cos^2\varphi\right) + \left(\sin^2\theta\sin^2\varphi\right)}{r^2}\right)\right)\right\}\frac{e^{-jkr}}{4\pi}, \quad (A.22)$$

$$E_{zz}^{\mathrm{ED}}(r,\theta,\varphi) = -j\frac{\omega u}{4\pi r}\frac{e^{-jkr}}{4\pi r}\sin^2\theta. \quad (A.23)$$

With a dipole current of Il, (A.17) is same as (A.3). This implies that the Cartesian copolar component $E_{xx}^{\mathrm{ED}}(r,\theta,\varphi)$ of x-directed electric point dipole derived through the far field

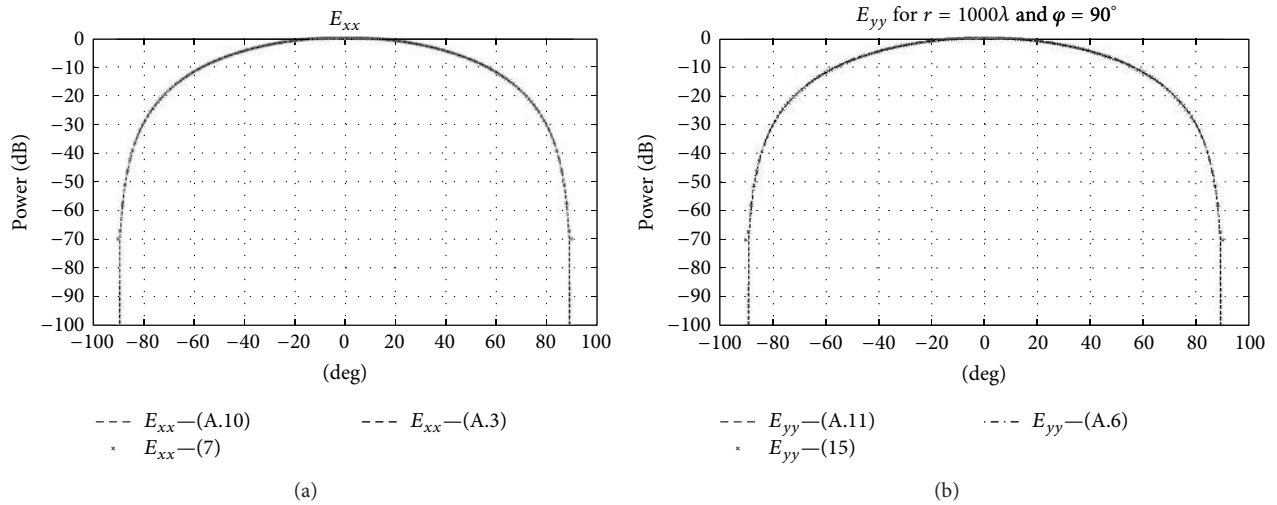

FIGURE 25: (a) Comparison of copolar (E_{xx}) component of x-directed electric point dipole in $\varphi = 0^\circ$ plane; $\lambda = 3.2$ cm. (b) Comparison of copolar (E_{yy}) component of y-directed electric point dipole in $\varphi = 90^\circ$ plane; $\lambda = 3.2$ cm.

simplification of expression (7) is identically equal to the one derived through alternate standard expressions of [11, page 155] and (A.17). Similarly, the Cartesian copolar component $E_y(r, \theta, \varphi)$ of y-directed electric point dipole derived through the far field simplification of expression (15) is identically equal to the one derived through alternate standard expression of [11, page 155] and (A.20). The same argument is valid for the copolar component of z-directed electric point dipole in view of the identical expressions involved in (A.9) and (A.23). From the above, it is easy to conclude that the proposed formulations of this paper for the near field radiation patterns of x-directed, y-directed, and z-directed electric point dipoles can be reduced to more compact form for the far field computations. To keep the paper concise, the aforementioned discussions have been restricted only to the Cartesian copolar components of electric point dipoles. To retain the generality of the presented analysis, expressions for the far field Cartesian cross polar components of electric point dipoles are also provided in this appendix. Based on the far field analysis of electric point dipoles, the far field (both co- and cross polar) components of magnetic dipoles can be derived using the well-known concept of duality.

The far field Cartesian components of x-directed electric point dipole are

$$\begin{aligned} E_{yx}^{\mathrm{ED}}(x,y,z,r) &= j\frac{\omega u}{r^3} yx \frac{e^{-jkr}}{4\pi}, \\ E_{zx}^{\mathrm{ED}}(x,y,z,r) &= j\frac{\omega u}{r^3} zx \frac{e^{-jkr}}{4\pi}, \\ H_{xx}^{\mathrm{ED}}(x,y,z,r) &= 0, \\ H_{yx}^{\mathrm{ED}}(x,y,z,r) &= (1+jk)\frac{-z}{r^2}\frac{e^{-jkr}}{4\pi}, \\ H_{zx}^{\mathrm{ED}}(x,y,z,r) &= (1+jk)\frac{y}{r^2}\frac{e^{-jkr}}{4\pi}. \end{aligned} \tag{A.24}$$

For a y-directed electric point dipole, the far field Cartesian components are

$$\begin{aligned} E_{xy}^{\mathrm{ED}}(x,y,z,r) &= j\omega u \frac{xy}{r^3}\frac{e^{-jkr}}{4\pi}, \\ E_{zy}^{\mathrm{ED}}(x,y,z,r) &= j\omega u \frac{zy}{r^3}\frac{e^{-jkr}}{4\pi}, \\ H_{yy}^{\mathrm{ED}}(x,y,z,r) &= 0, \\ H_{zy}^{\mathrm{ED}}(x,y,z,r) &= (1+jk)\frac{-x}{r^2}\frac{e^{-jkr}}{4\pi}, \\ H_{xy}^{\mathrm{ED}}(x,y,z,r) &= (1+jk)\frac{z}{r^2}\frac{e^{-jkr}}{4\pi}. \end{aligned} \tag{A.25}$$

The co- and cross polar components of a z-directed electric point dipole are

$$\begin{aligned} E_{zz}^{\mathrm{ED}}(x,y,z,r) &= \left\{-j\left(\frac{\omega u}{r}\left(\frac{x^2+y^2}{r^2}\right)\right)\right\}\frac{e^{-jkr}}{4\pi}, \\ E_{xz}^{\mathrm{ED}}(x,y,z,r) &= j\omega u \frac{xz}{r^3}\frac{e^{-jkr}}{4\pi}, \\ E_{yz}^{\mathrm{ED}}(x,y,z,r) &= j\omega u \frac{yz}{r^3}\frac{e^{-jkr}}{4\pi}, \\ H_{zz}^{\mathrm{ED}}(x,y,z,r) &= 0, \\ H_{yz}^{\mathrm{ED}}(x,y,z,r) &= (1+jk)\frac{-x}{r^2}\frac{e^{-jkr}}{4\pi}, \\ H_{xz}^{\mathrm{ED}}(x,y,z,r) &= (1+jk)\frac{y}{r^2}\frac{e^{-jkr}}{4\pi}. \end{aligned} \tag{A.26}$$

One of the novelties of the formulation presented in this paper for the computation of radiation patterns of electric and

magnetic dipoles is that the equations are valid for both near field and far field observation points. In essence it suffices to say the equations for the near field radiation patterns of this paper reduce to the far field equations of dipole derived through the formulations available in [11]. To demonstrate this feature, the far field copolar radiation patterns have been computed for x-directed and y-directed electric point dipoles with the source located at the origin using the following formulations:

(1) (A.3) and (A.6) for far field of electric point dipole derived through standard far field formulations of [11];

(2) modified equations (A.17) and (A.20) valid only for the far field;

(3) generic equations (7) and (15) which are uniformly valid for both near field and far field distances with $r = 1000\lambda$ to simulate a far field criterion.

As can be seen from the results of Figures 25(a) and 25(b), there is an excellent agreement between the simulation results derived through the three different formulations. The established agreement in the results of Figures 25(a) and 25(b) conclusively proves that the derived generic near field equations for radiation patterns of point dipoles reduce (or converge) to conventional far field equations for radiation patterns of point dipoles.

Conflict of Interests

The authors declare that there is no conflict of interests regarding the publication of this paper.

References

[1] S. Silver, *Microwave Antenna Theory and Design*, McGraw Hill Book, 1st edition, 1984.

[2] M. S. Narasimhan and K. S. Rao, "GTB analysis of the near-field patterns of conical and corrugated horns," *IEEE Transactions on Antennas and Propagation*, vol. 27, no. 5, pp. 705–708, 1979.

[3] M. S. Narasimhan, K. Raghavan, and P. Ramanujam, "A correction to the available formula for the GTD near field patterns of conical horns," *IEEE Transactions on Antenna and Propagation*, vol. 30, no. 5, pp. 1042–1043, 1982.

[4] M. S. Narasimhan and B. Philips, "Synthesis of near-field patterns of arrays," *IEEE Transactions on Antennas and Propagation*, vol. 35, no. 2, pp. 212–218, 1987.

[5] M. S. Narasimhan and P. Kumar, "A technique of synthesizing the excitation currents of planar arrays or apertures," *IEEE Transactions on Antennas and Propagation*, vol. 38, no. 9, pp. 1326–1332, 1990.

[6] M. Karthikeyan and K. R. Govind, *Near Field Radiation Patterns of Point Dipoles, Private Communication*, Centre for Systems and Devices, Indian Institute of Technology, Madras, India, 1985.

[7] R. A. Kennedy, D. B. Ward, and T. D. Abhayapala, "Nearfield beamforming using radial reciprocity," *IEEE Transactions on Signal Processing*, vol. 47, no. 1, pp. 33–40, 1999.

[8] R. A. Kennedy, T. D. Abhayapala, and D. B. Ward, "Broadband nearfield beamforming using a radial beampattern transformation," *IEEE Transactions on Signal Processing*, vol. 46, no. 8, pp. 2147–2156, 1998.

[9] M. S. Narasimhan and B. V. Rao, "Modes in a conical horn: new approach," *Proceedings IEE*, vol. 118, no. 2, pp. 287–292, 1971.

[10] R. F. Harrington, *Time-Harmonic Electromagnetic Fields*, McGraw-Hill, New York, NY, USA, 1961.

[11] H. Mott, *Polarization in Antennas and Radar*, John Wiley & Sons, Hoboken, NJ, USA, 1996.

[12] C. A. Balanis, *Antenna Theory, Analysis and Design*, John Wiley & Sons, New York, NY, USA, 3rd edition, 2005.